Environmental Pollution 268 (2021) 115794

Contents lists available at ScienceDirect

Environmental Pollution

journal homepage: www.elsevier.com/locate/envpol

Direct and cross impacts of upwind emission control on downwind $PM_{2.5}$ under various NH_3 conditions in Northeast Asia☆

Eunhye Kim [a], Byeong-Uk Kim [b], Hyun Cheol Kim [c, d], Soontae Kim [a, *]

[a] Department of Environmental & Safety Engineering, Ajou University, Suwon, South Korea
[b] Georgia Environmental Protection Division, Atlanta, GA, 30354, USA
[c] Air Resources Laboratory, National Oceanic and Atmospheric Administration, College Park, MD, 20740, USA
[d] Cooperative Institute for Satellite Earth System Studies, University of Maryland, College Park, MD, 20740, USA

ARTICLE INFO

Article history:
Received 28 February 2020
Received in revised form
10 September 2020
Accepted 6 October 2020
Available online 12 October 2020

Keywords:
Particulate matter
Upwind
Downwind
Emissions control
Long-range transport

ABSTRACT

Emissions reductions in upwind areas can influence the $PM_{2.5}$ concentrations in downwind areas via long-range transport. However, few studies have assessed the impact of upwind $PM_{2.5}$ precursor controls on changes in downwind $PM_{2.5}$ concentrations. In this study, we analyzed the overall impact of $PM_{2.5}$ precursor emission controls in upwind areas on $PM_{2.5}$ in downwind areas with two types of impacts: "direct impact" and "cross impact." The former refers to $PM_{2.5}$ changes in downwind areas due to the transported $PM_{2.5}$ itself, whereas the latter represents $PM_{2.5}$ changes due to reactions between the transported gaseous precursors and intermediates (i.e., HNO_3) originating from upwind areas and locally emitted precursors (i.e. NH_3) in the downwind areas. As a case study, we performed air quality modeling for Northeast Asia for January 15–17, 2016 by setting China and South Korea as the upwind and downwind areas, respectively. To account for potential spatiotemporal variations in NH_3 emissions in downwind areas, we considered two NH_3 conditions. When NOx emissions in China were reduced by 35%, in downwind areas the $PM_{2.5}$ concentrations decreased by 2.2 $\mu g/m^3$ under NH_3-rich conditions, while $PM_{2.5}$ concentrations increased by 2.3 $\mu g/m^3$ under NH_3-poor conditions. The direct impact increased by 4.0 $\mu g/m^3$ in both cases due to upwind NO_x disbenefit effects. However, the cross impacts led to a $PM_{2.5}$ decrease of 6.2 $\mu g/m^3$ under NH_3-rich conditions versus a $PM_{2.5}$ increase of 1.7 $\mu g/m^3$ under NH_3-poor conditions. We noted that $PM_{2.5}$ concentrations in the downwind areas may not improve unless a cross impact outweighs a direct impact. This may be one of the reasons why South Korea $PM_{2.5}$ concentrations have not declined despite efforts by China to reduce their $PM_{2.5}$ precursor emissions.

1. Introduction

Adverse health effects of particulate matter with an aerodynamic diameter smaller than or equal to 2.5 μm ($PM_{2.5}$), including cardiovascular and respiratory diseases, have been recognized as major public health threats (Chen et al., 2018; Ebenstein et al., 2017; Han et al., 2018; Lin et al., 2018). Global $PM_{2.5}$ pollution is associated with 4.2 million premature deaths each year (WHO, 2016). Thus, many countries set and enforce $PM_{2.5}$ air quality standards to reduce acute and chronic health risks due to short- and long-term exposure to high $PM_{2.5}$ concentrations (USEPA, 2013; WHO, 2016). In particular, short-term $PM_{2.5}$ exposure is often reported to cause emergency hospital visits and mortality (Li et al., 2019; Qiu et al., 2020; Yitshak et al., 2015). Short-term $PM_{2.5}$ air quality standards aim to ensure public health in areas that experience relatively high $PM_{2.5}$ concentrations and very short-term (e.g., several hours) $PM_{2.5}$ exposures (USEPA, 2013).

In Northeast Asia, short-term (e.g., daily) $PM_{2.5}$ standards have been exceeded frequently in recent years (An et al., 2019; Pei et al., 2018; Zou et al., 2017). One characteristic of short-term high (e.g., >35 $\mu g/m^3$, the national ambient air quality standard in South Korea for 24 h mean $PM_{2.5}$) $PM_{2.5}$ events in Northeast Asia is high contents of secondary inorganic aerosols (SIAs) detected in the total $PM_{2.5}$ concentration (Bae et al., 2020a; Huang et al., 2014; Itahashi et al., 2017; Kim et al., 2017a; Zhang et al., 2012). Because SIAs are formed via a series of atmospheric chemical reactions of their precursors (e.g., SO_2, NO_x, and NH_3), the reduction of SIA precursors will likely result in less frequent high $PM_{2.5}$ events (Pinder et al.,

☆ This paper has been recommended for acceptance by Admir C. Targino.
* Corresponding author.
E-mail address: soontaekim@ajou.ac.kr (S. Kim).

https://doi.org/10.1016/j.envpol.2020.115794

2007; Qu et al., 2016).

Therefore, each country in Northeast Asia has developed its own air quality improvement policies to reduce the number of times that the short-term $PM_{2.5}$ standards are exceeded. For example, China has been implementing the 13th Future Year Plan for 2016–2020 to control $PM_{2.5}$ precursors, including SO_2 and NO_x (China State Council, 2016). Sun et al. (2018) reported that the Chinese government aimed to decrease SO_2 and NOx emissions by 15% during the 13th Five-Year Plan (2016–2020). Cai et al. (2017) expected the emissions of SO_2 and NOx for 2012 to decrease by 40% and 44%, respectively, by 2020 in the Beijing–Tianjin–Hebei (BTH) region of China. Japan has also been reducing NO_x and NH_3 emissions in conjunction with its climate change policy (Ministry of the Environment, 2018; Wakamatsu et al., 2013). For South Korea, Kim et al. (2018) expected the emissions of SO_2 and NOx to decrease by 26% and 37%, respectively, during the comprehensive plan (2015–2022).

However, domestic controls alone will not work as intended because $PM_{2.5}$ precursor emissions in upwind regions can affect concentrations in downwind areas via long-range transport (Choi et al., 2019; Itahashi et al., 2017; Kim et al., 2017a, 2017b; Qu et al., 2016; Shimadera et al., 2016). Countries in downwind areas that experience considerable impacts of secondary $PM_{2.5}$ due to upwind emissions must understand how $PM_{2.5}$ precursors emitted and transported from upwind areas are converted to $PM_{2.5}$ in the downwind areas (USEPA, 2016).

Two major $PM_{2.5}$ precursors, SO_2 and NO_x, are primarily emitted into ambient air through fossil fuel combustion processes. They form H_2SO_4 and HNO_3 via atmospheric chemical reactions (Seinfeld and Pandis, 2006). These acidic gases are further converted into major SIAs, such as $(NH_4)_2SO_4$ and NH_4NO_3, after neutralization with NH_3 (Seinfeld and Pandis, 2006). Because NH_3 plays a critical role in SIA formation (Gu et al., 2014; Pinder et al., 2004, 2007; Yin et al., 2018), understanding NH_3 conditions in downwind areas is indispensable for accurately evaluating the effects of $PM_{2.5}$ precursor emission controls in upwind areas on improving $PM_{2.5}$ pollution in downwind areas. Thus, coordinated $PM_{2.5}$ precursor control strategies across multiple countries that incorporate environmental characteristics (e.g., NH_3 conditions) of upwind/downwind areas are necessary to establish effective $PM_{2.5}$ management. For example, European nations have improved their transboundary $PM_{2.5}$ pollution through collaborative efforts such as the Convention on Long-range Transboundary Air Pollution in 1979 and the Gothenburg Protocol in 1999 (Reis et al., 2012). Similar efforts will be needed in Northeast Asia to alleviate transboundary $PM_{2.5}$ pollution. However, few studies have been conducted that assess the impacts of $PM_{2.5}$ precursor controls in upwind areas on $PM_{2.5}$ changes in downwind areas by considering the complexities of $PM_{2.5}$ issues in Northeast Asia.

In this study, we performed a series of simulations using the Community Multi-scale Air Quality (CMAQ) model (Byun and Schere, 2006) to analyze $PM_{2.5}$ that is transported to and formed locally within downwind areas, in conjunction with a reduction in $PM_{2.5}$ precursor emissions in upwind areas. Specifically, we developed experimental scenarios that simultaneously consider $PM_{2.5}$ precursor controls in upwind areas and NH_3 conditions in downwind areas. We attempted to emphasize two major aspects of downwind $PM_{2.5}$ responses to upwind $PM_{2.5}$ precursor changes due to: (1) $PM_{2.5}$ transported from upwind areas and (2) interactive impacts between $PM_{2.5}$ precursors from upwind areas and those in downwind areas.

2. Methodology

2.1. Modeling domain and period

Because of prevailing westerly winds in Northeast Asia, China often plays the role of the upwind area, while Japan and South Korea become downwind areas. We defined the modeling domain for this study with a 27 km horizontal grid resolution to include all major upwind and downwind areas (Fig. 1). A choice of horizontal grid resolution for the photochemical grid model simulation may change the dilution of air pollutants emitted into the atmosphere, and thus the physiochemical processes that occur during transport. The 27 km grid resolution may be too coarse to detect urban or local conditions (i.e., the BTH region or near Beijing (NRB)). However, Gan et al. (2016) reported that the importance of grid resolution was relatively low for long-range transport case. Bae et al. (2020b) showed that differences in foreign emission impacts appreciated approximately 4% when 27 km and 9 km grid simulations were applied in Northeast Asia. Therefore, we applied a 27 km horizontal grid resolution in this study.

Bae et al. (2020a) showed that the observed $PM_{2.5}$ concentrations increased in the cold months during 2012–2016. They also mentioned that NO_3^- becomes a dominant $PM_{2.5}$ component during the winter months, while SO_4^{2-} is dominant during warm months. According to Bae et al. (2020a), Chinese emission impacts on NO_3^- in the Seoul Metropolitan Area were as high as 50% and 67% during the winter and spring, respectively. Bae et al. (2020b) also explained that Chinese emission impacts on the province-level $PM_{2.5}$ in South Korea during 2010–2017 had an annual mean ranging from 40 to 53%. However, the impact was as high as 60% during cold months. On the contrary, the foreign impact during the summer months was as low as 40% when the southwesterly winds became dominant.

Considering high ambient temperatures (>25 °C) and seasonal monsoons in Northeast Asia during the summer months, the transboundary transport influence of NH_4NO_3 on $PM_{2.5}$ concentrations becomes weak during the warm season. However, SO_2 emissions in China have reduced since 2006 due to the Chinese emissions control policy (Schreifels et al., 2012), which may increase the importance of long-range NH_4NO_3 transport in Northeast Asia, even during cold months.

Considering results from previous studies, the upwind impact on downwind NO_3^- becomes critical for determining the overall level of $PM_{2.5}$ during the cold months when the observed daily mean $PM_{2.5}$ frequently exceeds the National Ambient Air Quality Standard (NAAQS). We chose January 2016 as the modeling period because South Korea experienced very high $PM_{2.5}$ events in this period, likely due to $PM_{2.5}$ and its precursors transported from upwind areas (Park et al., 2018). In this period, the daily average $PM_{2.5}$ concentrations in South Korea ranged from 11 to 57 $\mu g/m^3$ (with a monthly average of ~30 $\mu g/m^3$) and the daily $PM_{2.5}$ standard (35 $\mu g/m^3$) was exceeded on 9 days (National Institute of Environmental Research (NIER), 2016). A 48 h HYSPLIT back-trajectory cluster analysis indicated that 52% of the airshed originated from the BTH and NRB areas (See Supplementary Fig. 1). Therefore, we concluded that the modeling period is suitable for this study.

2.2. Meteorological modeling

To develop meteorological inputs, we used Weather Research and Forecasting (WRF) v3.5.1 (Skamarock et al., 2008), with initial

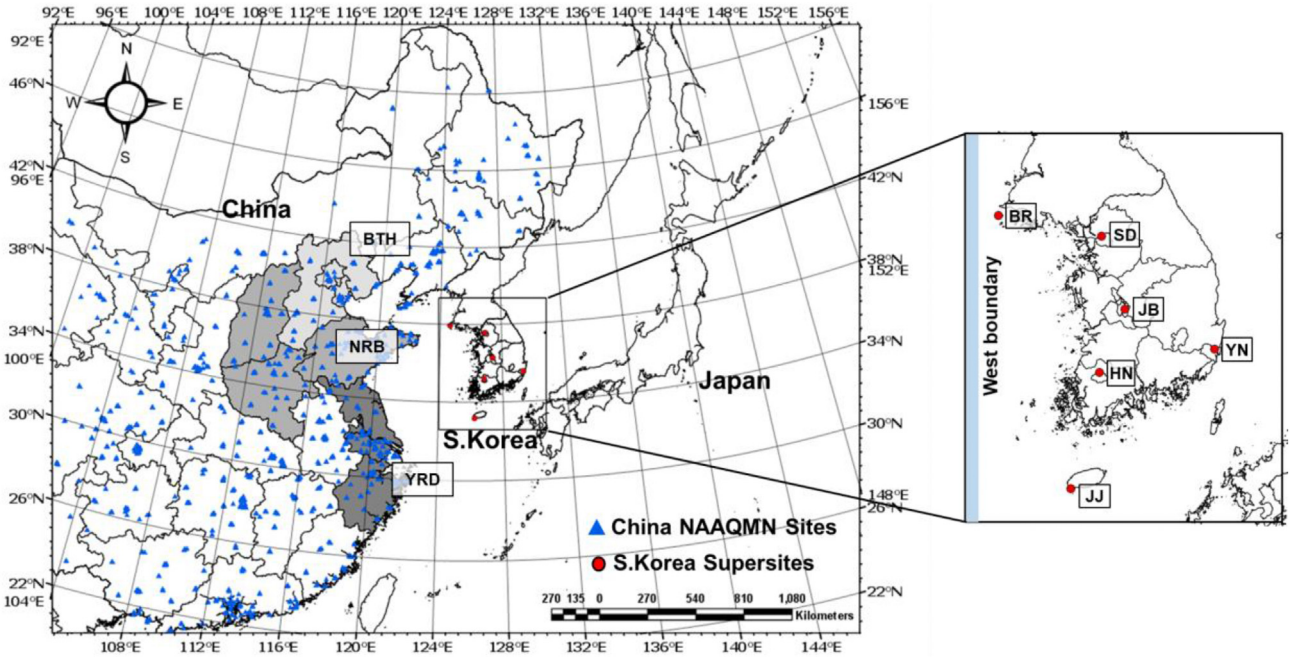

Fig. 1. Modeling domain and observational sites. Symbols indicate the locations of observation sites.

and boundary conditions derived from the Final Operational Global Analysis data from the National Centers for Environmental Prediction (NCEP). We processed the WRF outputs with the Meteorology–Chemistry Interface Processor (MCIP) v3.6 (Otte and Pleim, 2010) to prepare the CMAQ-ready meteorological input files. The height of the 1st vertical layer was approximately 32 m above ground level (AGL). The top of the vertical layers was located at 50 hPa (~20 km AGL). There were 22 vertical layers in total. Detailed information regarding the WRF configurations is presented in Supplementary Table 1. Because we focused on the effects of emission changes, we used one WRF simulation for all subsequent air quality modeling cases in this study.

2.3. Emissions inputs and modeling

The biogenic emissions model used in this study was prepared using the Model of Emissions of Gases and Aerosols from Nature (MEGAN) v2.04 (Guenther et al., 2006). Anthropogenic emissions were prepared using the Sparse Matrix Operator Kernel Emission (SMOKE) v3.1 (Benjey et al., 2001), for spatial and temporal allocations.

In terms of emission inventories for regions in Northeast Asia besides South Korea, we used the Comprehensive Regional Emissions inventory for the Atmospheric Transport Experiment (CREATE) 2015 (Woo et al., 2020). In this inventory, the annual NH_3 emissions in China are 12 Tg, which is 20% larger than the most frequently used emission inventory in the Chinese Multi-resolution Emission Inventory for China (MEIC) v1.0 (http://www.meicmodel.org/) modeling study. On the contrary, a monthly NH_3 emission rate in CREATE 2015 for January is 0.4 Tg/month, which is 50% of in the inventory used in MEIC v1.0. Considering a monthly allocation of annual total emissions, we reviewed the NH_3 emissions data for January, which is the modeling period of this study. The Magnitude and Seasonality of Agricultural Emissions (MASAGE) (Paulot et al., 2014) and a study by Huang et al. (2012) reported that monthly NH_3 emission rates for January in China are 0.3 Tg/month and 0.5 Tg/month, respectively. In addition, Zhang et al. (2018a) estimated that the January NH_3 emission rate in China could be 0.4 Tg/month, based on their top-down approach using satellite observations. These estimates are similar to the value used in this study for January (0.4 Tg/month). Discrepancies in the January NH_3 emission rates between MEIC v1.0 and all other data sources, including CREATE 2015, are probably due to the underestimation of temporal variability in agricultural activities in MEIC v1.0. Finally, to reflect SO_2 emission changes that occurred between the representing year of existing emission inventories (i.e., 2015) and the modeling year in this study (i.e., 2016), we reviewed the available emission inventories for 2015 and adjusted the existing emissions in the model (See Supplementary Fig. 2 for details).

For anthropogenic emissions in South Korea, we used the Clean Air Policy Support System (CAPSS) 2013 (http://airemiss.nier.go.kr/mbshome/mbs/airemiss/index.do), which is the official South Korean emission inventory. In the CAPSS, agriculture was responsible for 79% of total NH_3 emissions, followed by industrial processes (12%) and transportation (3%). Selective catalytic reduction (SCR) facilities accounted for 33% of industrial NH_3 emissions, and SCR equipped on diesel vehicles (i.e., trucks and buses) emitted 4% of NH_3 from the transportation sector. Previous studies conducted in South Korea have barely considered variability in the monthly NH_3 emission rates throughout a year (e.g. Choi et al., 2018; Kim et al., 2008). However, the monthly Northeast Asian NH_3 emission rates during the winter were estimated to be lower than 50% of those during the spring and summer (Huang et al., 2012; Paulot et al., 2014; Zhang et al., 2018a). Therefore, we assumed that the monthly South Korean NH_3 emissions in January can be overestimated twofold if a realistic temporal profile was not applied to CAPSS. Because NH_3 emissions reflecting the monthly variability can affect the modeled $PM_{2.5}$ including SIA, we applied two NH_3 emission scenarios (i.e., 100% and 50% of the existing emission rates) to account for any potential uncertainties in monthly NH_3 emission rates in South Korea when using CAPSS 2013.

2.4. Air quality simulation

For $PM_{2.5}$ air quality simulations, we used the CMAQ v4.7.1 model, with meteorological and emission inputs as described in previous sections. Details about the CMAQ setup in this study are presented in Supplementary Table 2. For the modeling scenarios, we developed modeling cases (as shown in Table 1) with various combinations of model-ready emissions datasets. To clarify the experimental conditions of each modeling scenario, we used the labeling system for modeling cases in Table 1 as follows. To examine the effect of local NH_3 emission variability on the modeled $PM_{2.5}$ in downwind areas (i.e., South Korea), we performed simulations with two NH_3 emission scenarios for South Korea: 100% (labeled as "A") and 50% (labeled as "B") of the base case NH_3 emission rates. The suffixes "1" or "2" were used for the sensitivity modeling cases to indicate NOx reduction only ("1") or simultaneous reductions in SO_2 and NOx emissions ("2") based on previous studies (Cai et al., 2017; Ding et al., 2019; Wang et al., 2014; Zhang et al., 2019). For example, SENS_A1 is a modeling case that assumes a 35% reduction in Chinese NO_x only, compared to 2016, and a monthly NH_3 emission rate in South Korea consistent with 100% of CAPSS 2013 without considering temporal variability of NH_3 emissions. While developing SO_2 and NOx emission scenarios for the set of model sensitivity simulations, we considered two aspects: (1) rich NH_3 conditions in Northeast Asia (Sung et al., 2020; Zhang et al., 2018b), and (2) relatively high sensitivity of NOx-to-NO_3^- conversion to NH_3 conditions, as compared to the SO_2-to-SO_4^{2-} conversion. For the latter, we assumed that secondary SO_4^{2-} formation is not limited unless NH_3 emissions are reduced by more than 50% of that in the base simulation, as shown in Section 2.5. Thus, we employed A1 and B1 to examine only NOx emission reduction cases, and A2 and B2 to estimate the simultaneous reductions in SO_2 and NOx emissions. On top of recent efforts in SO_2 emission reductions in China, we presumed that future NOx emission reductions in the country are inevitable.

2.5. "Overall," "direct," and "cross" impacts

To assess the effects of upwind control on downwind $PM_{2.5}$ concentrations using the various modeling scenarios, we compared the base case model (CNTR_A) results with sensitivity modeling results. $PM_{2.5}$ concentration differences between the base case model and sensitivity modeling of downwind areas (i.e. "impacts") represent an overall effect of precursor emission controls in the upwind areas on air quality changes in the downwind areas. We defined this overall effect as an "overall impact." We consider that an overall impact is essentially a sum of two types of impacts operationally defined as follows. A "direct impact" is a $PM_{2.5}$ concentration change made in upwind areas that propagates directly to downwind areas (i.e., without interaction with downwind emissions). Thus, by definition, a direct impact assumes no influence of chemical conditions in the downwind areas. To minimize the potential interference of downwind emissions on the quantitative assessment, we modeled direct impacts by averaging vertical cell concentrations from the ground to approximately 1 km AGL over the West boundary cells (Fig. 1) of South Korea. In contrast, a "cross impact" is a $PM_{2.5}$ concentration change due to the formation of $PM_{2.5}$ via chemical reactions between the transported $PM_{2.5}$ precursors, intermediates (such as HNO_3) from upwind areas, and $PM_{2.5}$ precursors emitted locally in the downwind areas. For this study, we defined the difference between an overall impact and a direct impact as a "cross impact." We used the term "cross" because the downwind SIAs are heavily influenced by oxidant conditions, nonlinear photochemical reactions in downwind areas, and abundances of SIA precursors or intermediates. Even though this operationally defined cross impact cannot be used to separately distinguish a variable domestic impact due to the different domestic NH_3 conditions from an overall impact, it can be used to assess bulk $PM_{2.5}$ responses in downwind areas to upwind emissions changes at various downwind NH_3 conditions. In summary, the cross impact, or the difference between an overall impact and a direct impact, can be considered the sum of a foreign indirect impact and a domestic indirect impact.

3. Results

3.1. Model performance evaluation

3.1.1. Meteorological model performance

To evaluate the performance of the meteorological model, we used observational data from available Meteorological Assimilation Data Ingest System (MADIS) sites (33 sites in China and 26 in South Korea). During January 2016, average 2 m temperatures were 1.0 °C (bias: 0.16 °C) and −1.6 °C (bias: −0.47 °C) in upwind and downwind areas, respectively. In addition, average 10 m wind speeds were 3.0 m/s (bias: 0.32 m/s) in upwind areas and 2.9 m/s (bias: 0.89 m/s) in downwind areas. For 2 m temperatures and 10 m wind speeds, the index of agreement (IOA) values ranged from 0.88 to 0.99. Model performances for the surface temperatures and winds were well within the benchmark suggested by Emery et al. (2001). Overall performance statistics are presented in Supplementary Table 3.

3.1.2. Air quality model performance

For air quality model performance evaluation, we compared the CNTR_A modeling results with measurements from National Ambient Air Quality Monitoring Network sites in China and supersites in South Korea (Fig. 1). There are 6 supersites operated by NIER in South Korea; Baengnyeong (BR), Sudo (SD), Jungbu (JB), Honam (HN), Yeongnam (YN), and Jeju (JJ). NIER provides hourly observations of $PM_{2.5}$, ionic species (SO_4^{2-}, NO_3^-, NH_4^+, etc.), carbonaceous species (EC, OC), and elemental constituents (Bae et al.,

Table 1
NOx, SO_2, and NH_3 emissions scenarios for the upwind and downwind areas.

	Upwind (China[1])	Downwind (South Korea[2])
CNTR_A (Base)	Base run[3]	EI-based simulation
SENS_A1	Sensitivity simulation with 35% reduction of NO_x emissions from CNTR_A	
SENS_A2	Sensitivity simulation with 35% reduction of SO_2 and NO_x emissions from CNTR_A	
CNTR_B	CTM-based control run[3]	50% reduction in NH_3 emission rate in corresponding "A" cases
SENS_B1	Sensitivity simulation with 35% reduction of NO_x emissions from CNTR_B	
SENS_B2	Sensitivity simulation with 35% reduction of SO_2 and NO_x emissions from CNTR_B	

1 Adjusted CREATE 2015 emissions inventory is used for Chinese emissions.
2 CAPSS 2013 emissions inventory is used for Korean emissions.
3 Simulation with 35% reduction of SO_2 emissions from EI.

2020a, 2020b; Jo et al., 2020; Kim et al., 2017a).

We examined modeling accuracies for the entire month of January for the modeling domain. Spatially, we focused on BTH and NRB because their impacts on South Korea have been deemed significant. Supplementary Table 4 (see also Supplementary Fig. 3) shows $PM_{2.5}$ overprediction in BTH (i.e., a normalized mean bias (NMB) of 25.5% and a fractional bias (FB) of 29.5%) and underprediction in NRB (i.e., a NMB of −17.7% and a FB of 13.8%). BTH was the upwind area during the episode, which can be connected to an overprediction of the upwind impact. Several reasons are possible for the model behaviors: model algorithms and representation, uncertainties in emissions, and meteorological input data. However, we assumed that the effect of the overprediction was reduced after long-range transport of air pollutants (Gan et al., 2016). Moreover, the simulation satisfied the statistical benchmarks including the NMB, normalized mean error (NME), Pearson correlation coefficient (R), FB, and fractional error (FE) proposed by Emery et al. (2017) and Boylan and Russell (2006). In addition, the simulated daily mean SIA concentrations for Baengnyeong, South Korea were compared to the observations (Supplementary Fig. 4 and Supplementary Table 5). Baengnyeong Island (37.9648°N, 124.6340°E) is located in northwesternmost South Korea and is close to North Korea. This site is considered downwind of China and upwind of South Korea. In January 2016, the observed daily mean concentrations of SO_4^{2-}, NO_3^-, and NH_4^+ were 2.36 ± 2.93 (0.56–14.17) (mean ± standard deviation (minimum–maximum)) μg/m^3, 2.95 ± 5.19 (0.19–23.10) μg/m^3, and 1.76 ± 2.88 (0.10–12.91) μg/m^3, respectively, while the simulated concentrations were 1.79 ± 1.33 (0.84–5.91) μg/m^3, 3.02 ± 2.98 (0.26–12.06) μg/m^3, and 1.53 ± 1.29 (0.50–5.12) μg/m^3. For China, we compared the simulated SIA concentrations to the values observed in a previous study by Sun et al. (2014). Simulated SO_4^{2-}, NO_3^-, and NH_4^+ concentrations in Beijing, China were 6.7 μg/m^3, 5.7 μg/m^3, and 4.2 μg/m^3 during the January 2016 episode. The observations from Sun et al. (2014) were 14.3 μg/m^3 for SO_4^{2-}, 12.5 μg/m^3 for NO_3^-, and 9.2 μg/m^3 for NH_4^+ in January 2013. Zhang et al. (2019) showed that the observed SO_4^{2-}, NO_3^-, and NH_4^+ in Beijing, China decreased by 52%, 25%, and 43%, respectively, between 2013 and 2017.

Organic carbon, as well as SIA, accounts for a major portion of $PM_{2.5}$ in Northeast Asia (Bae et al., 2020a; Ming et al., 2017; Uno et al., 2020). However, three-dimensional photochemical models still have difficulties representing observed organic carbon or organic matter (Bae et al., 2020a; Yin et al., 2017). Moreover, the role of volatile organic carbon emissions in secondary aerosol formation is quite underestimated (Yin et al., 2015) in Northeast Asia. Thus, we focused on SIA transport and transformation in this study. Previous studies have explained that the SIA portion increases during wintertime in Northeast Asia (Bae et al., 2020a; Huang et al., 2014; Itahashi et al., 2017).

Because this study focuses on assessing the impacts of upwind $PM_{2.5}$ precursor emission reductions on downwind $PM_{2.5}$ concentrations, we set January 15–17, 2016, as the analysis period. During this period, the daily $PM_{2.5}$ concentrations in South Korea were over 35 μg/m^3 (Supplementary Fig. 5; Supplementary Table 6). These high daily $PM_{2.5}$ concentrations might have resulted from more than 70% contributions from upwind areas (Supplementary Fig. 5) and the major contributing area was BTH (Supplementary Fig. 6).

3.2. Impacts of SO_2 and NOx emission changes on upwind $PM_{2.5}$

When Chinese NOx was reduced by 35% (SENS_A1), NO_3^- concentrations of all regions of China (including BTH) decreased by 15.5% on average, but the concentrations in BTH increased by 10.8% (Fig. 2, Supplementary Table 7). In the model, because BTH was under NOx-rich conditions, excessive NOx titrated O_3. NOx reduction in a NOx-rich area resulted in increased oxidant concentrations, such as O_3 (Fujita et al., 2013). In turn, the elevated oxidants in the upwind area rapidly produced more HNO_3. When sufficient NH_3 is available, the rapid HNO_3 formation prompts HNO_3-to-NO_3^- conversion over the upwind area (Cai et al., 2017; Huang et al., 2020; Kim et al., 2017d; Nguyen and Dabdub, 2002). This phenomenon is called "NO_x disbenefit" (Lee et al., 2006). In a previous study, Yang et al. (2019) reported that the recent increase of winter O_3 in Tianjin, China was due to decreased NO titration. Cai et al. (2017) also concluded that an increase of O_3 in China was caused by the reduction of NOx emissions. Supplementary Fig. 7 shows the January trend of observed NO_2 and O_3 concentrations in China and BTH from 2015 to 2018. From these observations, the monthly mean O_3 concentrations exhibit an obvious increasing trend, while NO_2 concentrations exhibit a decreasing trend during the same period. Lowered NO_2 concentrations represent NOx emission reductions over the areas, and thus reduced NO emissions resulted in reduced ozone titration. Therefore, we can conclude that NOx emission reductions in high NOx areas leads to reduced NO titration and increased O_3, even during the winter months. We confirmed that regions with high NO_x (such as BTH) exhibited increased O_3 concentrations compared to those without NOx emissions reductions (Supplementary Fig. 8). As shown in Fig. 3, the total N (=NO + NO_2+NO_3+HNO_3+HONO+$2N_2O_5$+PANs + NO_3^-) concentration in China, including BTH, decreased with Chinese NOx reductions, while the fraction of NO_3^- in the total N increased. Consistently, the nitrogen oxidation ratio (NOR = $[NO_3^-]$/($[NO_3^-]$ + $[NO_2]$)) (Sun et al., 2006) and the nitrate fraction in the total N from the vertical column density of regions in eastern China, such as BTH and Shanghai, also increased (Supplementary Figs. 9 and 10). However, it should be noted that NOx emission reduction in the upwind areas eventually decreased HNO_3 concentrations in the downwind areas.

When Chinese NO_x and SO_2 emissions were reduced simultaneously (e.g. SENS_A2), NO_3^- concentrations averaged over China decreased by 13.3%, which is similar to the case of NO_x reduction only (e.g. SENS_A1) (Figs. 2, 4 and Supplementary Table 7). When only NO_x reductions were made in China (e.g. SENS_A1), SO_4^{2-} concentrations over BTH and the Yellow Sea were 2 μg/m^3 higher than the base case (CNTR_A), as shown in Fig. 2. Similar to the process for NOx, SO_2 can be converted into SO_4^{2-} with an increase of oxidants when NO concentrations are reduced. SO_4^{2-} concentrations also increased in BTH by 0.52–0.84 μg/m^3, which was approximately half that of NO_3^-. Unlike the NO_3^- decrease (−1.51 μg/m^3) after the NOx emissions reductions, SO_2 emissions reductions increased the nationwide SO_4^{2-} concentrations by 0.32 μg/m^3, which compensates the NO_3^- decrease by 36% after the 35% upwind NOx emissions reduction. To explain this increase using chemistry, we utilized the Sulfur Tracking Model (STM) available in CMAQ. STM outputs include chemical change rates for each reaction pathway that the emitted SO_2 undergoes, such as chemical reaction pathways explaining the gas phase or aqueous phase oxidation of S (IV) to S (VI). STM analyses indicate that the increased SO_4^{2-} could be attributed to gas phase oxidation more than aqueous phase oxidation (Supplementary Figs. 11 and 12).

However, when both NO_x and SO_2 emissions were reduced (e.g. SENS_A2), SO_4^{2-} concentrations decreased in all regions in China except BTH (Fig. 4). Considering a purely NO_x reduction-led increase in SO_4^{2-}, we hypothesized that an overall decrease in the SO_4^{2-} concentration with simultaneous SO_2 and NO_x emission controls in China was likely due to stronger effects of SO_2 reduction than those of NO_x disbenefits. On the contrary, an increase in SO_4^{2-} concentrations in BTH was the result of the stronger effects of NO_x disbenefits than those of SO_2 reduction (Pinder et al., 2008a). After a 35% reduction in NOx emissions from China, NO_3^- and SO_4^{2-} were

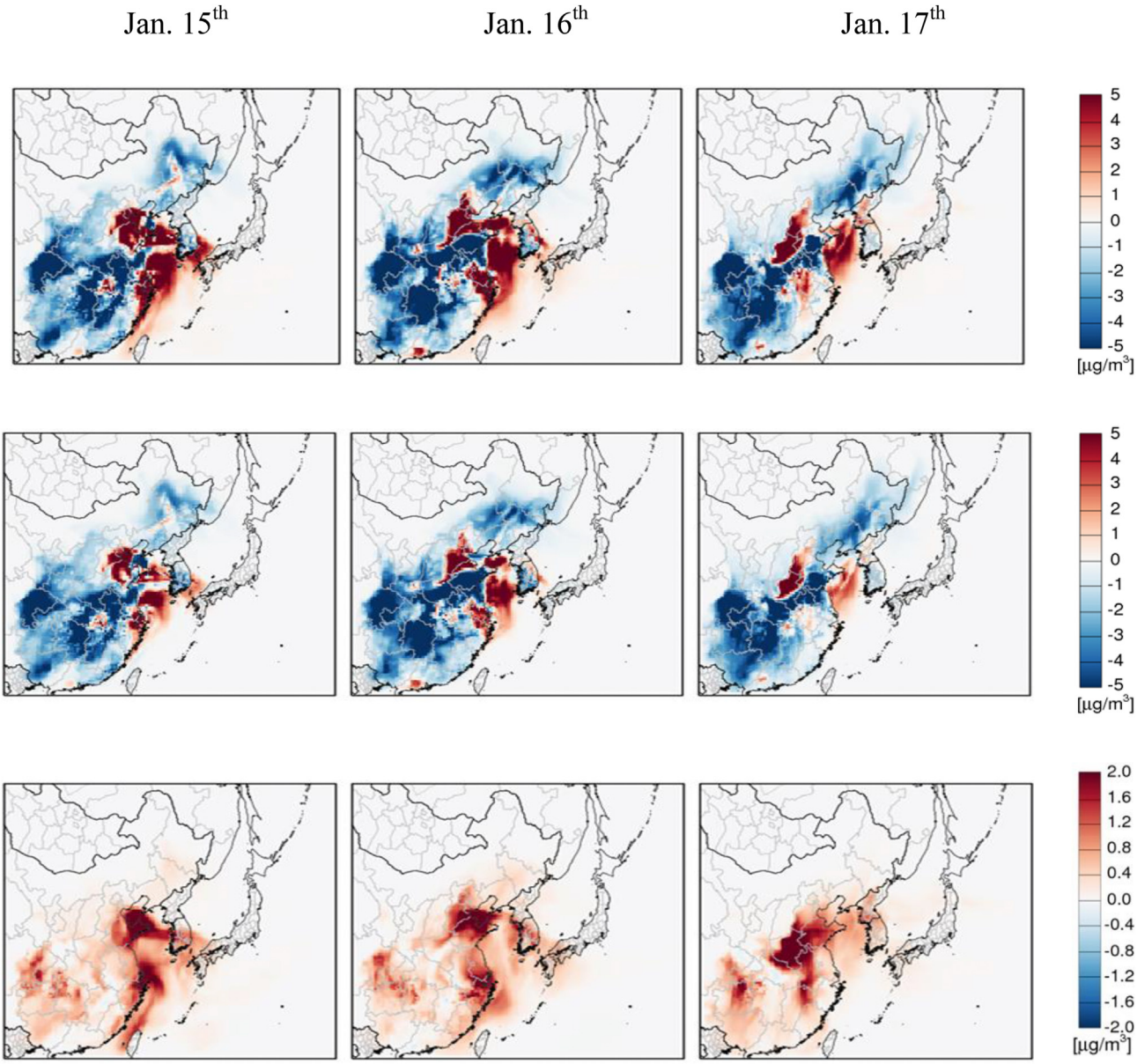

Fig. 2. Impact of Chinese NOx emission reductions (SENS_A1-CNTR_A) on regional $PM_{2.5}$ (top), NO_3^- (middle), and SO_4^{2-} (bottom) concentrations.

simulated to increase over high NOx emission areas and their downwind areas (i.e., BTH and Shanghai), as shown in Fig. 2. Meteorology might influence the formation and concentrations of secondary inorganic ions. It is also known that the difference in transformation rates of NO_3^- and SO_4^{2-} could cause slight spatial shifts. For example, Lachatre et al. (2019) explained that SO_2 oxidation processes are slower than NOx oxidation processes.

In summary, the reduction in SO_2 emissions in China led to a decrease in SO_4^{2-} levels in the country. On the contrary, the reduction in NO_x emissions resulted in spatially variable changes in NO_3^- (i.e., positive and/or negative) over China, as well as elevated SO_4^{2-} concentrations in and around BTH. For a 35% NO_x-only reduction (e.g., SENS_A1), $PM_{2.5}$ concentrations in China and BTH decreased by 1.39 μg/m^3 (3.5%) and increased by 2.92 μg/m^3 (2.6%), respectively. For 35% NO_x and SO_2 reductions (e.g. SENS_A2), $PM_{2.5}$ concentrations in China and BTH decreased by 1.99 μg/m^3 (5.0%) and 2.49 μg/m^3 (2.2%), respectively. Spatial variations of changes in NO_3^- due to NO_x disbenefits may drive the overall spatial variations of $PM_{2.5}$ changes.

Until recently, emission control policies in China focused on SO_2 emissions rather than NO_x emissions (Lachatre et al., 2019; Zheng et al., 2018). Since Chinese emissions of SO_2 had already decreased by 59% in 2017 compared to 2013 (Zhang et al., 2019), China can focus on the reduction of NOx emissions more than those of SO_2. However, when China starts implementing NOx-focused emission control strategies, the precursor controls may cause unintended aftereffects, such as the increases in $PM_{2.5}$ concentrations shown in this study. For example, a NO_x emission reduction in NO_x-rich areas such as BTH exhibited increases in $PM_{2.5}$ and its precursor concentrations. In turn, elevated $PM_{2.5}$ concentrations can be propagated to downwind areas via long-range transport, as illustrated by backward-trajectory analysis results.

3.3. Changes in $PM_{2.5}$ concentrations in downwind regions

When continental outflow in northeast Asia transports air

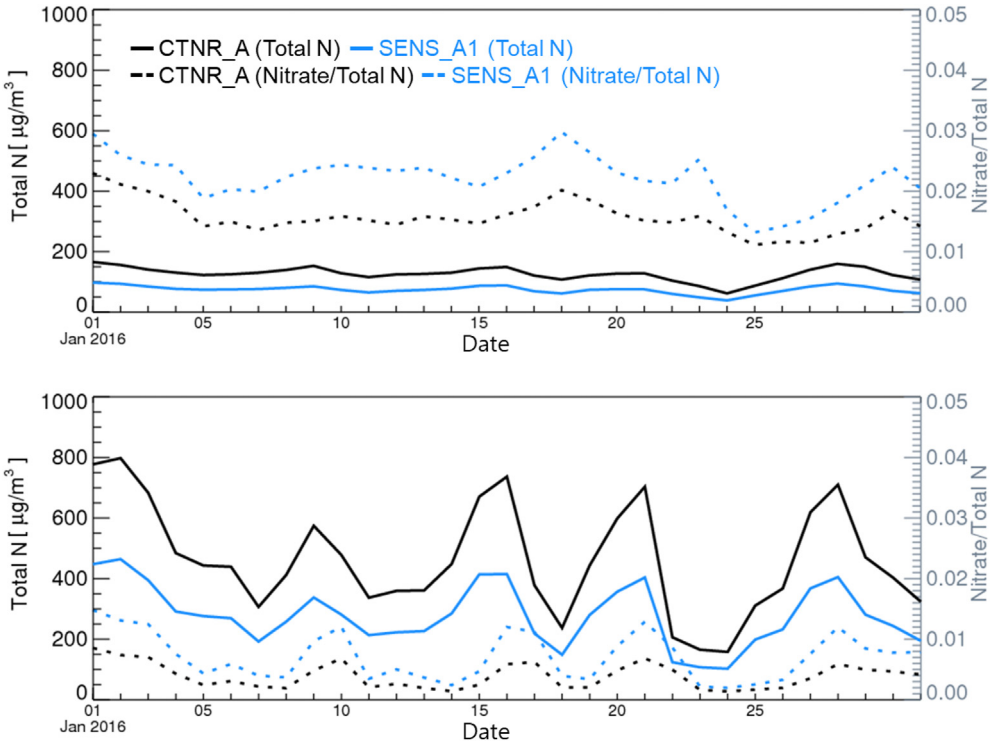

Fig. 3. Time series of total N concentrations and the fraction of NO_3^- over China (top) and BTH (bottom). Black lines represent the results of CNTR_A. Blue lines represent SENS_B. Solid and dotted lines represent total N and NO_3^-/total N, respectively. (For interpretation of the references to colour in this figure legend, the reader is referred to the Web version of this article.)

pollutants from China (an upwind area) to South Korea and Japan (downwind areas), Chinese air pollutants will likely cross the Yellow Sea (Bhardwaj et al., 2019). During our focused analysis period, the airshed originating from China crossed the Yellow Sea and entered South Korea (Supplementary Fig. 6). Thus, we set an influx estimation area over the Yellow Sea ("west boundary" in Fig. 1) and used changes in the concentrations of $PM_{2.5}$ and its components due to Chinese emissions changes at the west boundary as a proxy influx of $PM_{2.5}$ and its constituents to South Korea from China.

In Fig. 5(a), the west boundary represents the SENS_A1-CNTR_A case, which is nearly the same for the SENS_B1-CNTR_B case because the west boundary is not affected by changes in downwind emissions. Accounting for direct impact contributions, 35% Chinese NOx emission reductions during the focused analysis period increased the concentrations of $PM_{2.5}$ by 4.6 μg/m^3 (11%), NO_3^- by 2.5 μg/m^3 (40%), SO_4^{2-} by 0.8 μg/m^3 (18%), and NH_4^+ by 1.1 μg/m^3 (31%) at the west boundary in the simulation results (Fig. 5 (a)). Percentages within the parentheses are relative magnitudes of the changes in concentration estimated by CNTR_A. In addition, the maximum direct impacts on $PM_{2.5}$, NO_3-, SO_4^{2-}, and NH_4^+ during this period were as high as 5.4 μg/m^3, 3.2 μg/m^3, 1.0 μg/m^3, and 1.3 μg/m^3, respectively. However, the same emission reductions caused the HNO_3 concentrations to decrease by 7.0 μg/m^3 (54%) (Fig. 5 (a)). Before reaching the west boundary, changes in HNO_3 in upwind areas will be reflected in NO_3^- changes in upwind areas due to its rapid neutralization with NH_3, forming NH_4NO_3. We examined how HNO_3 is transported downwind using the Process Analysis Integrated Process Rate (PA IPR) (Supplementary Fig. 13). PA IPR is one of probing tools supported by CMAQ that allows the quantitative contributions of each process to be addressed (i.e., emission, advection, diffusion, chemical reaction, and deposition) for grid cells or areas of interest. The PA IPR shows that the dry deposition process decreases HNO_3 concentrations near the surface. On the contrary, horizontal advection and thermal decomposition of NH_4NO_3 increase HNO_3 concentrations in the lower atmosphere (~500 m). Conversely, the gas-to-aerosol conversion increases NO_3^- concentrations at altitudes between 500 and 1000 m (Supplementary Fig. 14). The model shows that the main provider of surface-level HNO_3 at the west boundary is the thermal decomposition of NH_4NO_3 during the focused analysis period.

HNO_3 is an intermediate species that can react with NH_3 to form NH_4NO_3 after being transported to downwind areas. Thus, HNO_3 is critical for explaining changes in downwind NO_3^- concentrations. Moreover, the conversion of HNO_3 transported from upwind areas to NO_3^- can be very sensitive to the availability of downwind NH_3. Considering these effects, we estimated that changes in $PM_{2.5}$ concentrations due to a 35% Chinese NOx reduction would be −0.1 μg/m^3 (−0.2%) (A) and 1.47 μg/m^3 (4.2%) (B) depending on the NH_3 conditions in South Korea.

In the following section, we describe changes in pollutant concentrations in downwind areas as "direct impacts" and "cross impacts." N_2O_5, which is another intermediate species, was not considered due to its negligible concentrations in our simulation (Supplementary Fig. 15).

To analyze the magnitudes of cross impacts with variable HNO_3 influxes, we estimated the NH_3 conditions in South Korea. To identify the NH_3 conditions, we adopted the adjusted gas ratio (AdjGR), which is the molar ratio of free ammonia to total nitrate (Eq. (1)) as proposed by Pinder et al. (2008b). If the AdjGR is greater than 1, the conditions can be considered NH_3-rich. If the AdjGR is less than 1, the conditions are defined as NH_3-poor.

$$AdjGR = \frac{[NH_3] + [NO_3^-]}{[NO_3^- + [HNO_3]]} \quad (1)$$

Because agriculture, livestock, and SCR are major anthropogenic

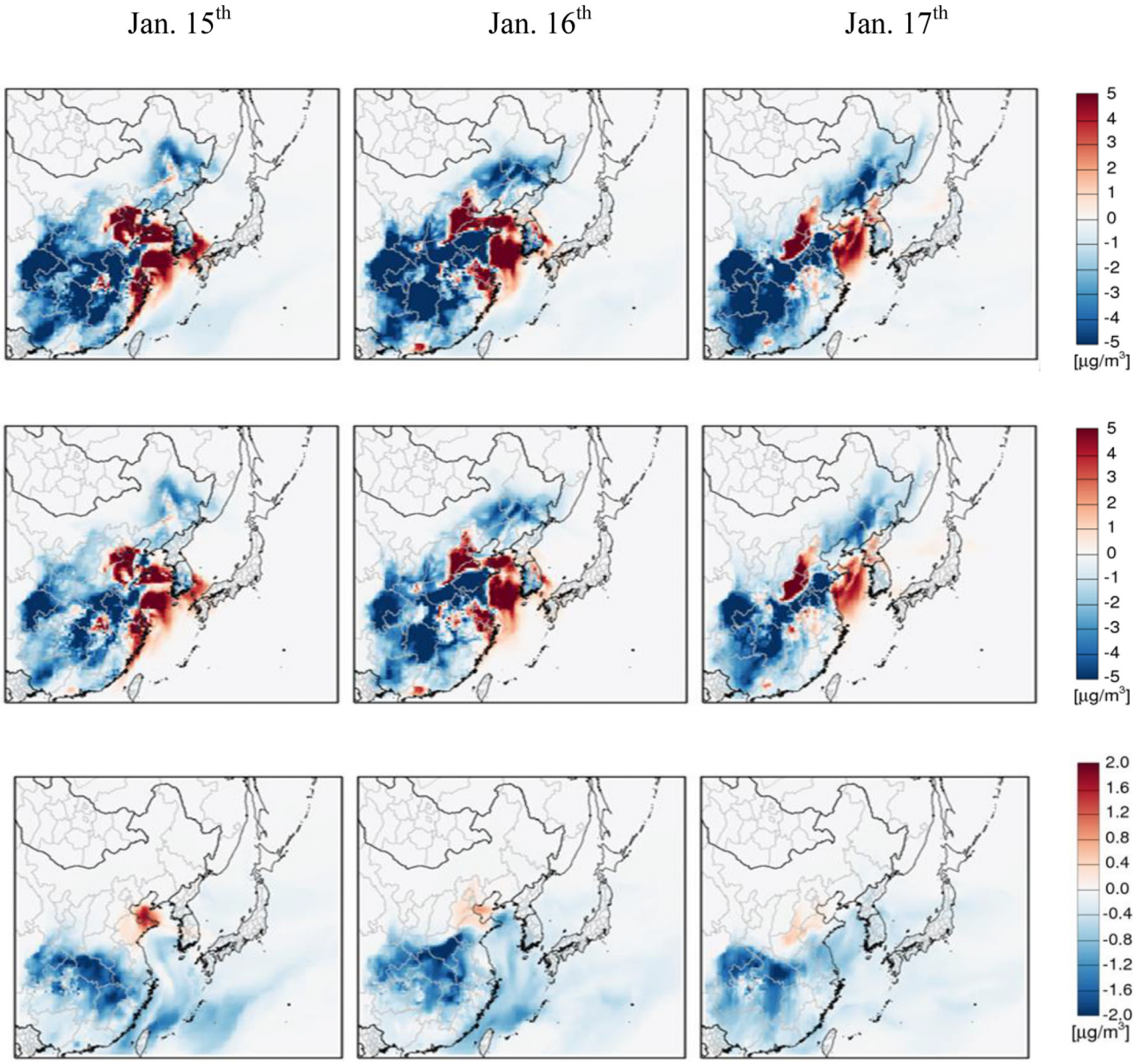

Fig. 4. Impacts of Chinese NOx and SO_2 emissions reductions (SENS_A2-CNTR_A) on regional $PM_{2.5}$, (top), NO_3^- (middle), and SO_4^{2-} (bottom) concentrations.

NH_3 emission sources in South Korea, we estimated the AdjGR over in-land modeling grid cells. A spatially averaged AdjGR value for the base case model (CNTR_A) was 1.1 (i.e., NH_3-rich conditions), while AdjGR values for CNTR_A in 46.5% of all land cells were less than 1 (i.e. NH_3-poor conditions). A spatially averaged AdjGR value for the downwind NH_3 sensitivity case with 50% NH_3 emissions (CNTR_B) was 0.7 (NH_3-poor conditions) and AdjGR values for CNTR_B in 72% of all land cells were less than 1 (NH_3-poor conditions). The spatial variability of NH_3-poor conditions due to NH_3 emission variability was estimated as 25.5% (Supplementary Fig. 16).

Thus, we classified the downwind areas using the results of the two modeling scenarios, CNTR_A and CNTR_B, to account for potential uncertainties in NH_3 conditions due to uncertainties in NH_3 emissions (Fig. 6). Region "R1" is located where downwind areas are under NH_3-rich conditions in CNTR_A and CNTR_B. Region "R2" is located where downwind areas are under NH_3-rich conditions in CNTR_A, but NH_3-poor conditions in CNTR_B. Region "R3" is located where downwind areas are under NH_3-poor conditions in CNTR_A and CNTR_B. By classifying the downwind areas into these three groups, we could minimize the effects of local characteristics and microscale variabilities (i.e., terrain, emissions other than NH_3, and meteorology) when we conducted analyses under various NH_3 conditions to derive more general conclusions.

Table 2 presents the $PM_{2.5}$ and SIA concentration changes in R1–R3 when Chinese NOx emissions were reduced. Overall, the impacts on NO_3^- concentrations decreased by 2.6 μg/m^3 (A) and 1.2 μg/m^3 (B) during the focused analysis period in R1. Considering that the direct NO_3^- impact in west boundary was 2.0 μg/m^3, the cross impact decreased by 4.6 μg/m^3 (A) and 3.2 μg/m^3 (B), respectively. At the same time, the impacts in R3 with a 35% Chinese NOx reduction during the focused analysis period increased by 0.2 μg/m^3 (A) and 0.9 μg/m^3 (B) while the cross NO_3^- impacts decreased by 1.8 μg/m^3 (A) and 1.1 μg/m^3 (B). For R3, the direct impact is greater than the cross impact under NH_3-poor conditions. The ratio of NO_3^- changes due to the direct and cross impacts was 1.8 (= 2.0/1.1).

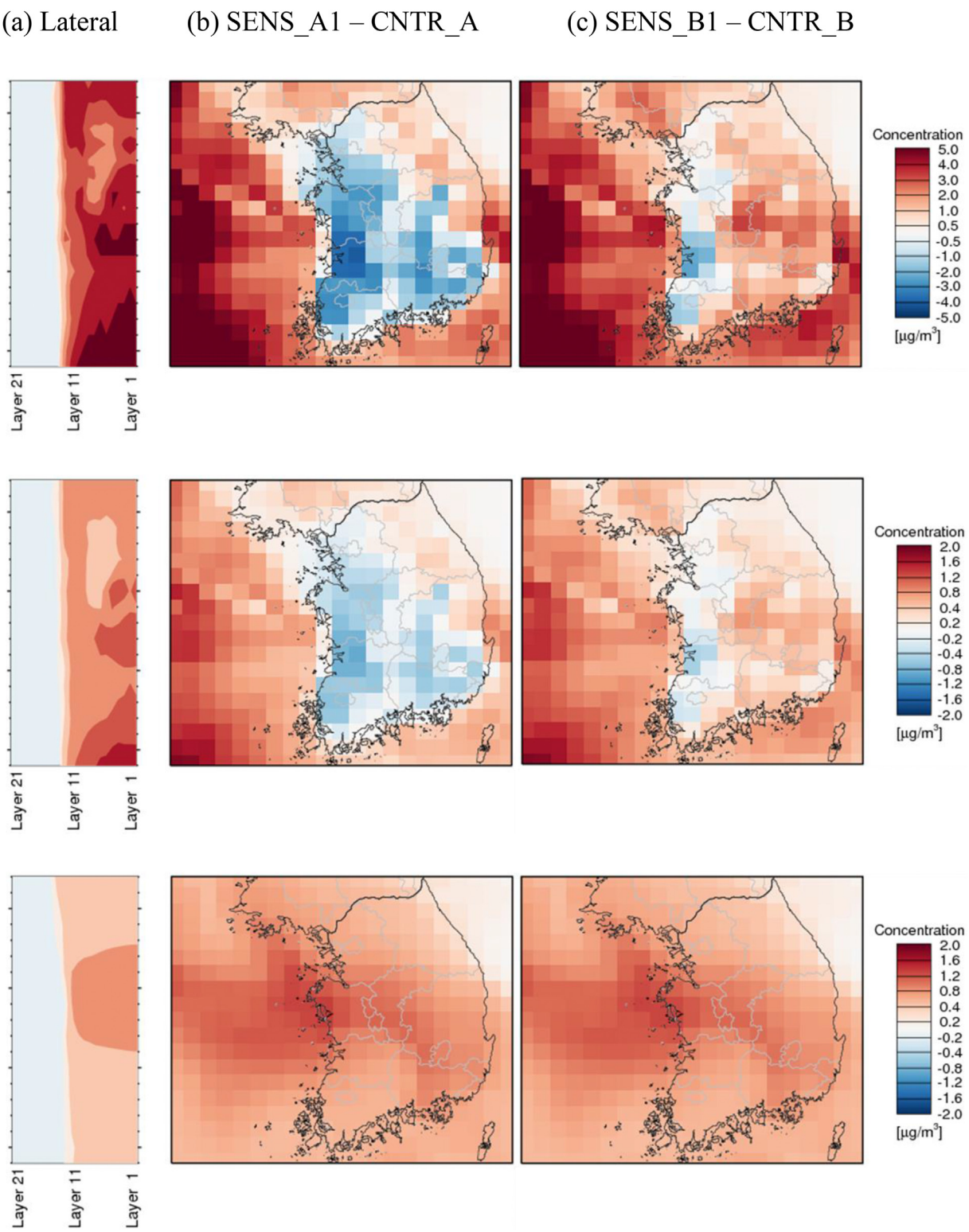

Fig. 5. Impact of 35% Chinese NO_x emissions on $PM_{2.5}$, NH_4^-, SO_4^{2-}, NO_3^-, and HNO_3: (a) direct impact, (b) overall impact with 100% NH_3 emissions (SENS_A1 − CNTR_A) in South Korea, and (c) overall impact with 50% NH_3 emissions (SENS_B1 − CNTR_B) in South Korea. The top of layers 11 and 21 correspond to 1 km and 10 km above sea level, respectively.

In R1, the magnitude of the cross impact was twice (=4.6/2.0) that of the direct impact. Unlike R1, R3 lacked available NH_3 to react with HNO_3. This means that NO_3^- formation in downwind areas was less sensitive to transported HNO_3 in R3 than in R1. In R2, the overall impact decreased by 2 μg/m^3 between SENS_A1 and CNTR_A, while little change in NO_3^- was estimated between SENS_B1 and CNTR_B. In other words, for the areas subject to large NH_3 emission uncertainties (in turn, uncertainties in NH_3-

conditions) such as R2 (i.e., NH_3-rich to NH_3-poor conditions), the relative importance of cross and direct impacts used to determine downwind NO_3^- concentrations can be also highly uncertain. Therefore, caution is warranted when interpreting modeling results. In addition, it is important to develop accurate NH_3 emissions models in the future.

Spatial distributions of regional NH_3-conditions in downwind areas, including NH_3 emission uncertainties (i.e., R1−R3), show that R1 (where NO_3^- concentrations decreased with Chinese NOx emission reductions) covers large cities, industrial complexes, and paddy fields (Fig. 5 (b), (c)), R2 (where NO_3^- concentrations increased between SENS_A1 and CNTR_A, while NO_3^- concentrations decreased between SENS_B1 and CNTR_B) encompasses suburban areas, and R3 (where NO_3^- concentrations increased with Chinese NOx emission reductions) includes islands and mountainous terrain. SO_4^{2-} concentrations changed little (<0.1 μg/m^3) with Chinese NOx reductions in R1−R3 at downwind areas. The gas-to-particle partitioning of SO_4^{2-} is irreversible; thus, the conversion rate of H_2SO_4 to SO_4^{2-} is relatively slower than that of NO_3^-. Therefore, during the analysis period, the changes in $PM_{2.5}$ concentrations in the downwind areas were primarily driven by changes in NO_3^- concentrations rather than SO_4^{2-} concentrations. For the modeling scenarios that contained simultaneous Chinese NOx and SO_2 reductions (SENS_A2 and SENS_B2), we did not present the direct or cross impacts here because changes in the $PM_{2.5}$ and HNO_3 concentrations at the west boundary (i.e., direct impact) were similar to those in SENS_A1 and SENS_B1.

Fig. 7 summarizes the key findings of this study. To clarify our findings, we denoted pollutants originating from upwind areas with "U" and those from downwind areas with "D." If NOx

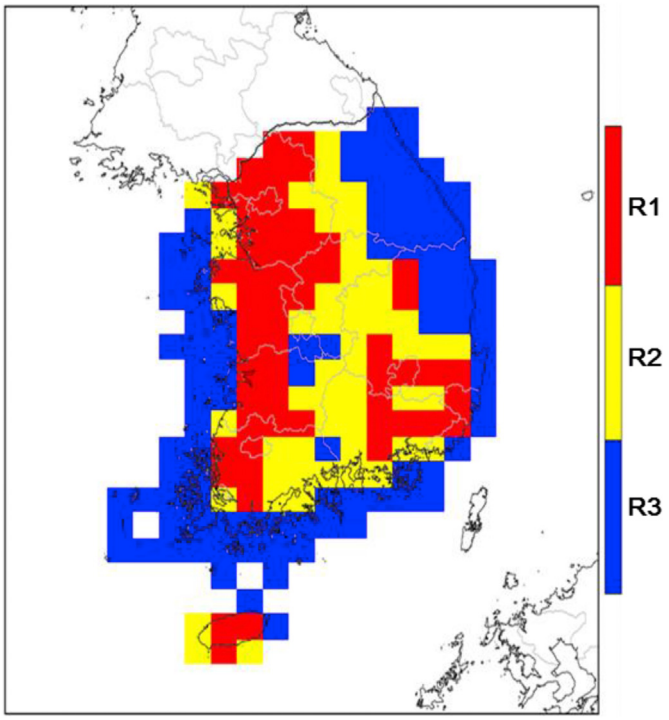

Fig. 6. Classified downwind areas in this study. R1 is NH_3-rich regions for CNTR_A and CNTR_B, R2 is NH_3-rich regions for CNTR_A and NH_3-poor regions for CNTR_B, and R3 is NH_3-poor regions for CNTR_A and CNTR_B.

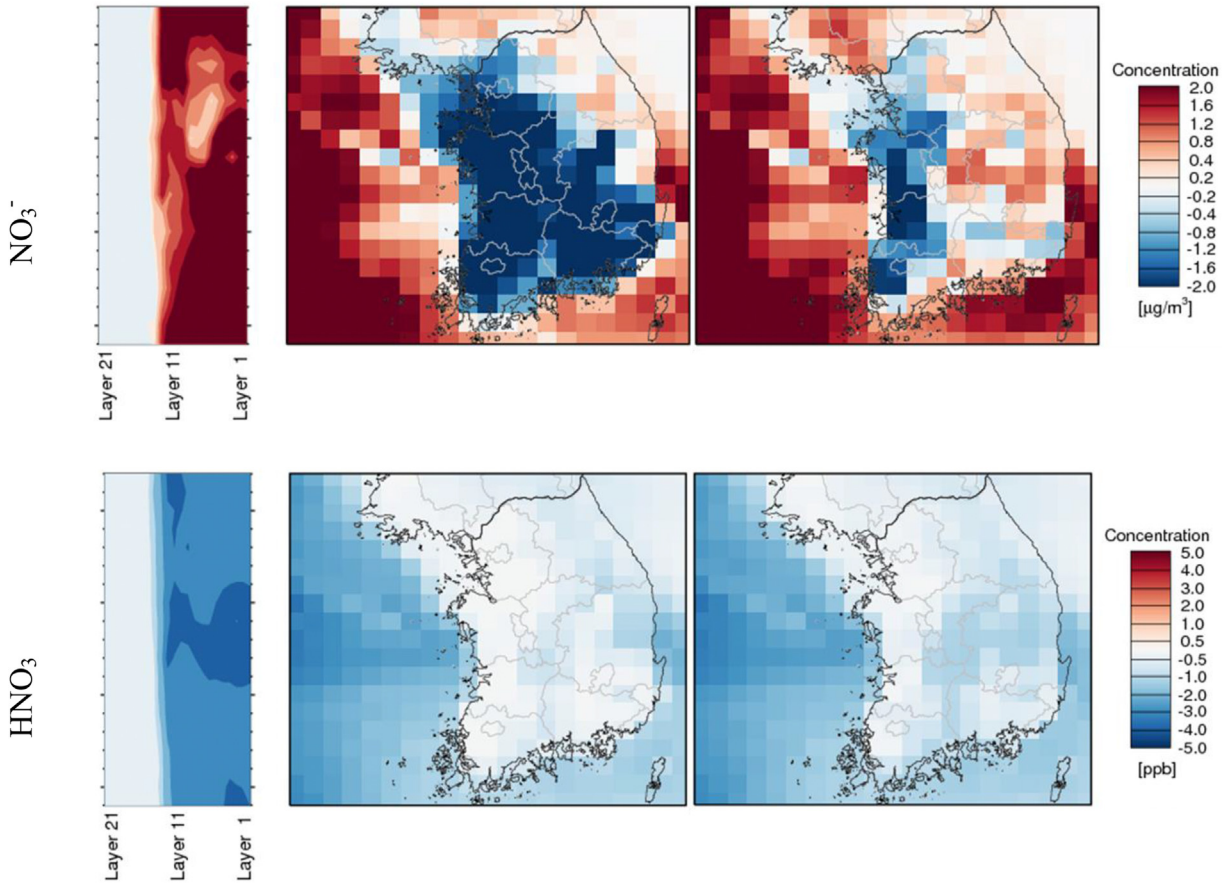

Fig. 5. (*continued*).

Table 2
Average overall, direct, and cross impacts due to a 35% Chinese NO_x emissions reduction, depending on NH_3 conditions in the downwind areas (units: μg/m^3).

		NO_3^-		NH_4^+		SO_4^{2-}		$PM_{2.5}$	
		A	B	A	B	A	B	A	B
Overall impact[1]	R1[4]	-2.6	-1.2	-0.5	-0.1	0.7	0.7	-2.2	-0.4
	R2[5]	-2.1	0.0	-0.3	0.3	0.8	0.8	-1.3	1.4
	R3[6]	0.2	0.9	0.4	0.5	0.7	0.7	1.4	2.3
Direct impact[2]	R1	2.0		1.0		0.7		4.0	
	R2								
	R3								
Cross impact[3]	R1	-4.6	-3.2	-1.5	-1.1	0.0	0.0	-6.2	-4.4
	R2	-4.1	-2.0	-1.3	-0.7	0.1	0.1	-5.3	-3.6
	R3	-1.8	-1.1	-0.6	-0.5	0.0	0.0	-2.6	-1.7

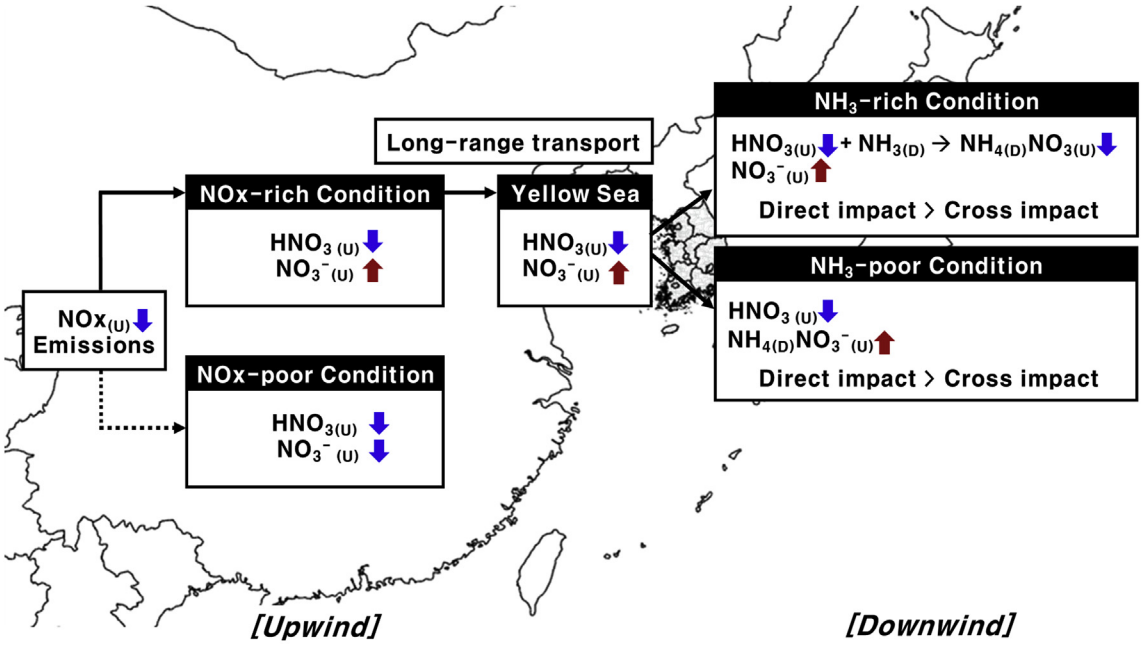

Fig. 7. Illustration of the propagated impacts of upwind NO_x emission reductions on downwind $PM_{2.5}$ based on downwind NH_3 conditions. "U" and "D" denote the origins (i.e. upwind vs. downwind) of the pollutants.

emissions in China were reduced, $NO_{3(U)}^-$ concentrations over most areas in China decreased, while NOx-rich areas such as BTH exhibited increased $NO_{3(U)}^-$ concentrations due to the NOx disbenefit effects. Overall effects of upwind NO_x emission reductions on the downwind NO_3^- concentrations can vary due to the relative contributions of $NO_{3(U)}^-$ and $HNO_{3(U)}$ transported from upwind areas (i.e., direct impact). Since $HNO_{3(U)}$ will react with $NH_{3(D)}$, changes in the $HNO_{3(U)}$ influx will cause changes in $NH_{4(D)}NO_{3(U)}^-$ concentrations, owing to reactions between $HNO_{3(U)}$ and $NH_{3(D)}$ (i.e., cross impact).

An analysis of the change in concentration at the west boundary during the analysis period (Jan. 15–17, 2016) shows increased $NO_{3(U)}^-$ and decreased $HNO_{3(U)}$ when Chinese NOx emissions were reduced. Increased $NO_{3(U)}^-$ influxes can contribute to an overall increase in NO_3 concentration ($= NO_{3(U)}^- + NO_{3(D)}^-$) in downwind areas. Decreased $HNO_{3(U)}$ influxes have mixed effects depending on the NH_3 conditions in the downwind areas. Under NH_3-rich conditions, a decreased $HNO_{3(U)}$ influx leads to less formation of

$NH_{4(D)}NO_{3(U)}$ (3.2–4.6 μg/m^3) in downwind areas (see Eq. (2)). In contrast, under NH_3-poor conditions, decreased $HNO_{3(U)}$ influx leads to smaller (1.6–2.3 μg/m^3) differences in overall NO_3^- concentrations in downwind areas than under NH_3-rich conditions because of less formation of $NH_{4(D)}NO_{3(U)}$ (see Eq. (3)).

NH_3 rich (HNO_3-limited): $HNO_{3(U)} \downarrow + NH_{3(D)} \rightarrow NH_{4(D)}NO_{3(U)} \downarrow$ (2)

NH_3 poor (NH_3-limited): $HNO_{3(U)} \downarrow +$ limited $NH_{3(D)} \rightarrow$ $NH_{4(D)}NO_{3(U)}$ change is limited. (3)

This means that NH_3-rich areas such as large cities (i.e. R1) will receive noticeable benefits of upwind NO_x controls, while NH_3-poor areas such as islands (i.e. R3) may see little benefit. However, it should be noted that this study examined a limited case, and several other factors (meteorological conditions and influx pathways) can affect changes in downwind $PM_{2.5}$ concentrations due to upwind precursor emission controls.

4. Conclusions

In this modeling study, we examined how the efficacy of $PM_{2.5}$ precursor emission controls in upwind areas changed $PM_{2.5}$ concentrations (including secondary inorganic aerosols) in downwind areas. As an illustrative case study, we chose Northeast Asia because China often plays the role of an upwind area, while South Korea becomes a downwind area during high $PM_{2.5}$ events in the region. We attempted to analyze air quality changes in the downwind areas according to upwind emission controls, i.e. "overall impact," with "direct" and "cross" impacts that we defined operationally. During the focused study period, the direct impact following Chinese $PM_{2.5}$ precursor controls was an increase in $PM_{2.5}$ concentrations due to elevated NO_3^- concentrations, which were due to the NOx disbenefit effect. We also showed that the cross impact is sensitive to NH_3 conditions in downwind areas and becomes more noticeable when local conditions are NH_3-rich, rather than NH_3-poor. This has significant air quality management implications for South Korea, because many of its large cities and industrial complexes are under NH_3-rich conditions and contain large NOx emitters. In general, increased SO_2 and NOx controls in China and South Korea will likely lead to the eventual reduction of high $PM_{2.5}$ events in South Korea. However, as we demonstrated in this study, an overall improvement in downwind $PM_{2.5}$ air quality (i.e. overall impact) will not be achieved until the magnitude of the negative direct impact (i.e., increased $PM_{2.5}$ in upwind areas) is less than that of the positive cross impact. This may partly explain why the South Korean $PM_{2.5}$ air quality has not improved significantly, even though China and South Korea have undertaken efforts to reduce their $PM_{2.5}$ precursor emissions. We conclude that the chemical environment over East Asia is very complex and pollutant problems in downwind countries are not easily explained without a careful understanding of the chemical conditions, implying that the efficiency of pollution mitigation efforts is affected not only by local governments, but also by close international collaboration. To reduce the uncertainties of the modeling study, we suggest two future research topics. First, as we noted in this study, uncertainties in NH_3 emissions need to be reduced. One way to achieve this is to determine NH_3 conditions based on NH_3 measurements. Second, to accurately quantify the direct and cross impacts, it is necessary to track physical (e.g. advection) and chemical (e.g. secondary inorganic aerosol formation) processes individually for major $PM_{2.5}$ intermediate species and precursors (e.g. HNO_3 and NH_3) from upwind and downwind areas with a suitable diagnostic analytical tool such as PA IPR.

Author statement

Eunhye Kim: Conceptualization, Investigation, Visualization, Writing - original draft, Byeong-Uk Kim: Conceptualization, Methodology, Writing - review & editing, Hyun Cheol Kim: Software, Writing - review & editing, Soontae Kim: Supervision

Declaration of competing interest

The authors declare that they have no known competing financial interests or personal relationships that could have appeared to influence the work reported in this paper.

Acknowledgements

This work was supported by the National Strategic Project-Fine Particle of the National Research Foundation of Korea (NRF) funded by the Ministry of Science and ICT (MSIT), the Ministry of Environment (ME), and the Ministry of Health and Welfare (MOHW) (2017M3D8A1092015) in South Korea.

Appendix A. Supplementary data

Supplementary data to this article can be found online at https://doi.org/10.1016/j.envpol.2020.115794.

References

An, Z., et al., 2019. Severe haze in northern China: a synergy of anthropogenic emissions and atmospheric processes. Proc. Natl. Acad. Sci. Unit. States Am. 116, 8657–8666.
Bae, C., et al., 2020a. Long-range transport influence on key chemical components of $PM_{2.5}$ in the Seoul metropolitan area, South Korea, during the years 2012–2016. Atmosphere 11, 48.
Bae, M., et al., 2020b. A multiscale tiered approach to quantify contributions: a case study of PM2.5 in South Korea during 2010–2017. Atmosphere 11, 141.
Bhardwaj, P., et al., 2019. Recent changes of trans-boundary air pollution over the Yellow Sea: implications for future air quality in South Korea. Environ. Pollut. 247, 401–409.
Benjey, W., et al., 2001. Implementation of the SMOKE Emission Data Processor and SMOKE Tool Input Data Processor in Models-3. US EPA.
Boylan, J.W., Russell, A.G., 2006. PM and light extinction model performance metrics, goals, and criteria for three-dimensional air quality models, Atmos. Environ. Times 40, 4946–4959.
Byun, D.W., Schere, K.L., 2006. Review of the governing equations, computational algorithms, and other components of the Models-3 Community Multiscale Air Quality (CMAQ) modeling system. Appl. Mech. Rev. 59 (2), 51–77.
Cai, S., et al., 2017. The impact of the 'air pollution prevention and control action plan' on PM 2.5 concentrations in Jing-Jin-Ji region during 2012–2020. Sci. Total Environ. 580, 197–209.
Chen, Y., et al., 2018. Estimating household air pollution exposures and health impacts from space heating in rural China. Environ. Int. 119, 117–124.
China State Council, 2016. The 13th Five-Year Plan on Energy Saving and Emissions Reduction. China State Council, Beijing, China.
Choi, J., et al., 2019. Impacts of local vs. trans-boundary emissions from different sectors on $PM_{2.5}$ exposure in South Korea during the KORUS-AQ campaign. Atmos. Environ. 203, 196–205.
Choi, K.-C., et al., 2018. Evaluation of the simulated $PM_{2.5}$ concentrations using air quality forecasting system according to emission inventories - focused on China and South Korea. KOSAE 34, 306–320.
Ding, A., et al., 2019. Significant reduction of PM 2.5 in eastern China due to regional-scale emission control: evidence from SORPES in 2011–2018. Atmos. Chem. Phys. 19, 11791–11801.
Ebenstein, A., et al., 2017. New evidence on the impact of sustained exposure to air pollution on life expectancy from China's Huai River Policy. Proc. Natl. Acad. Sci. Unit. States Am. 114, 10384–10389.
Emery, C., et al., 2001. Enhanced Meteorological Modeling and Performance Evaluation for Two Texas Ozone Episodes. Prepared for the Texas Natural Resource Conservation Commission. ENVIRON International Corporation.
Emery, C., et al., 2017. Recommendations on statistics and benchmarks to assess photochemical model performance. J. Air Waste Manag. Assoc. 67 (5), 582–598.
Fujita, E.M., et al., 2013. Past and future ozone trends in California's South Coast Air Basin: reconciliation of ambient measurements with past and projected emission inventories. J. Air Waste Manag. Assoc. 63, 54–69.
Gan, C.-M., et al., 2016. Assessment of the effects of horizontal grid resolution on long-term air quality trends using coupled WRF-CMAQ simulations. Atmos.

Environ. 132, 207–216.
Gu, B., et al., 2014. Agricultural ammonia emissions contribute to China's urban air pollution. Front. Ecol. Environ. 12, 265–266.
Guenther, A., et al., 2006. Estimates of global terrestrial isoprene emissions using MEGAN (model of emissions of gases and aerosols from nature). Atmos. Chem. Phys. 6 (11), 3181–3210.
Han, C., et al., 2018. Spatial and temporal trends of number of deaths attributable to ambient PM 2.5 in Korea. KOSAE 33.
Huang, R.-J., et al., 2014. High secondary aerosol contribution to particulate pollution during haze events in China. Nature 514, 218–222.
Huang, X., et al., 2012. A high-resolution ammonia emission inventory in China: ammonia Emission in China. Global Biogeochem. Cycles 26 (1).
Huang, X., et al., 2020. Enhanced secondary pollution offset reduction of primary emissions during COVID-19 lockdown in China. Natl. Sci. Rev. nwaa137.
Itahashi, S., et al., 2017. Nitrate transboundary heavy pollution over East Asia in winter. Atmos. Chem. Phys. 17, 3823–3843.
Jo, Y.-J., et al., 2020. Changes in inorganic aerosol compositions over the Yellow Sea area from impact of Chinese emissions mitigation. Atmos. Res. 240, 104948.
Kim, B.-U., et al., 2017a. Spatially and chemically resolved source apportionment analysis: case study of high particulate matter event. Atmos. Environ. 162, 55–70.
Kim, E., et al., 2018. Evaluation of the effectiveness of emission control measures to improve $PM_{2.5}$ concentration in South Korea. KOSAE 34, 469–485.
Kim, H.C., et al., 2017b. Regional contributions to particulate matter concentration in the Seoul metropolitan area, South Korea: seasonal variation and sensitivity to meteorology and emissions inventory. Atmos. Chem. Phys. 17, 10315–10332.
Kim, S., Moon, N., Byun, D.W., 2008. Korea emissions inventory processing using the EPA's SMOKE system. AJAE 2–1, 34–36.
Kim, S., et al., 2017d. PM 2.5 Simulations for the Seoul metropolitan area: (I) Contributions of precursor emissions in the 2013 CAPSS emissions inventory. KOSAE 33, 139–158.
Lachatre, M., et al., 2019. The unintended consequence of SO_2 and NO_2 regulations over China: increase of ammonia levels and impact on $PM_{2.5}$ concentrations. Atmos. Chem. Phys. 19, 6701–6716.
Lee, S., et al., 2006. Estimation of the seasonal variation of particulate nitrate and sensitivity to the emission changes in the greater Seoul area. Atmos. Environ. 40, 3724–3736.
Li, T., et al., 2019. Estimating mortality burden attributable to short-term PM2.5 exposure: A national observational study in China. Environ. Int. 125, 245–251.
Lin, H., et al., 2018. Daily exceedance concentration hours: a novel indicator to measure acute cardiovascular effects of $PM_{2.5}$ in six Chinese subtropical cities. Environ. Int. 111, 117–123.
Ministry of the Environment, 2018. Government of Japan. https://www.env.go.jp/press/pm2.5_9/mat7.pdf.
Ming, L., et al., 2017. $PM_{2.5}$ in the Yangtze River Delta, China: chemical compositions, seasonal variations, and regional pollution events. Environ. Pollut. 223, 200–212.
National Institute of Environmental Research (NIER), 2016. Annual Report of Air Quality in Korea.
Nguyen, K., Dabdub, D., 2002. NOx and VOC control and its effects on the formation of aerosols. Aerosol Sci. Technol. 36, 560–572.
Otte, T.L., Pleim, J.E., 2010. The meteorology–chemistry interface processor (MCIP) for the CMAQ modeling system: updates through MCIPv3.4.1, Geosci. Model Dev 3 (1), 243–256.
Park, Y., et al., 2018. Characterizing isotopic compositions of TC-C, NO3−-N, and NH4+-N in $PM_{2.5}$ in South Korea: impact of China's winter heating. Environ. Pollut. 233, 735–744.
Paulot, F., et al., 2014. Ammonia emissions in the United States, European Union, and China derived by high-resolution inversion of ammonium wet deposition data: interpretation with a new agricultural emissions inventory (MASAGE_NH_3). J. Geophys. Res. Atmos. 119, 4343–4364.
Pei, L., et al., 2018. Increasing persistent haze in Beijing: potential impacts of weakening East Asian winter monsoons associated with northwestern Pacific sea surface temperature trends. Atmos. Chem. Phys. 18, 3173–3183.
Pinder, R.W., Adams, P.J., Pandis, S.N., 2007. Ammonia emission controls as a cost-effective strategy for reducing atmospheric particulate matter in the eastern United States. Environ. Sci. Technol. 41, 380–386.
Pinder, R.W., et al., 2004. A process-based model of ammonia emissions from dairy cows: improved temporal and spatial resolution. Atmos. Environ. 38, 1357–1365.
Pinder, R.W., Gilliland, A.B., Dennis, R.L., 2008a. Environmental impact of atmospheric NH_3 emissions under present and future conditions in the eastern United States: future impact of NH3 emissions. Geophys. Res. Lett. 35, 12.
Pinder, R.W., Dennis, R.L., Bhave, P.V., 2008b. Observable indicators of the sensitivity of $PM_{2.5}$ nitrate to emission reductions—Part I: derivation of the adjusted gas ratio and applicability at regulatory-relevant time scales. Atmos. Environ. 42, 1275–1286.
Qiu, X., et al., 2020. Inverse probability weighted distributed lag effects of short-term exposure to $PM_{2.5}$ and ozone on CVD hospitalizations in New England Medicare participants – exploring the causal effects. Environ. Res. 182, 109095.
Qu, Y., et al., 2016. An overview of emissions of SO_2 and NO_x and the long-range transport of oxidized sulfur and nitrogen pollutants in East Asia. J. Environ. Sci. 44, 13–25.
Reis, S., et al., 2012. From acid rain to climate change. Science 338, 1153–1154.
Schreifels, J.J., et al., 2012. Sulfur dioxide control in China: policy evolution during the 10th and 11th Five-year Plans and lessons for the future. Energy Pol. 48, 779–789.
Seinfeld, J.H., Pandis, S.N., 2006. Atmospheric Chemistry and Physics – from Air Pollution to Climate Change, third ed. John Wiley & Sons, New York, USA.
Sun, Y., et al., 2014. Investigation of the sources and evolution processes of severe haze pollution in Beijing in January 2013: Sources and Evolution of Haze Pollution. J. Geophys. Res. Atmos. 119, 4380–4398.
Sun, W., et al., 2018. Long-term trends of anthropogenic SO_2, NO_x, CO, and NMVOCs emissions in China. Earth's Future 6, 1112–1133.
Shimadera, H., et al., 2016. Evaluation of air quality model performance for simulating long-range transport and local pollution of PM 2.5 in Japan. Adv. Meteorol. 2016, 1–13.
Skamarock, W.C., et al., 2008. A time-split nonhydrostatic atmospheric model for weather research and forecasting applications. J. Comput. Phys. 227, 3465–3485.
Sun, Y., et al., 2006. Chemical characteristics of PM 2.5 and PM 10 in haze–fog episodes in Beijing. Environ. Sci. Technol. 40, 3148–3155.
Sung, M., et al., 2020. A long term trend of gaseous and particulate acid/base species and effects of ammonia reduction on nitrate contained in $PM_{2.5}$, 2009~2018. KOSAE 36, 249–261.
Uno, I., et al., 2020. Paradigm shift in aerosol chemical composition over regions downwind of China. Sci. Rep. 10, 6450.
USEPA, 2013. Air Quality: EPA's 2013 Changes to the Particulate Matter (PM) Standard.
USEPA, 2016. Cross-state Air Pollution Rule Update for the 2008 Ozone NAAQS.
Wakamatsu, S., et al., 2013. Air pollution trends in Japan between 1970 and 2012 and impact of urban air pollution countermeasures. AJAE 7 (4).
Wang, S.X., et al., 2014. Emission trends and mitigation options for air pollutants in East Asia. Atmos. Chem. Phys. 14 (13), 6571–6603.
Woo, J.-H., et al., 2020. Development of the CREATE inventory in support of integrated climate and air quality modeling for Asia. Sustainability 12 (7930).
World Health Organization (WHO), 2016. Ambient Air Pollution.
Yang, J., et al., 2019. Study of the meteorological influence on ozone in urban areas and their use in assessing ozone trends in all seasons from 2009 to 2015 in Tianjin, China. Meteorol. Atmos. Phys. 131, 1661–1675.
Yin, S., et al., 2015. A refined 2010-based VOC emission inventory and its improvement on modeling regional ozone in the Pearl River Delta Region, China. Sci. Total Environ. 514, 426–438.
Yin, S., et al., 2018. Characteristics of inorganic aerosol formation over ammonia-poor and ammonia-rich areas in the Pearl River Delta region, China. Atmos. Environ. Times 177, 120–131.
Yin, X., et al., 2017. Source contributions to $PM_{2.5}$ in Guangdong province, China by numerical modeling: results and implications. Atmos. Res. 186, 63–71.
Yitshak, S.M., et al., 2015. Air pollution and ischemic stroke among young adults. Stroke 46, 3348–3353.
Zhang, H., et al., 2012. Source apportionment of $PM_{2.5}$ nitrate and sulfate in China using a source-oriented chemical transport model. Atmos. Environ. 62, 228–242.
Zhang, L., et al., 2018a. Agricultural ammonia emissions in China: reconciling bottom-up and top-down estimates. Atmos. Chem. Phys. 18, 339–355.
Zhang, Y., et al., 2018b. The vertical variability of ammonia in urban Beijing, China. Atmos. Chem. Phys. 18, 16385–16398.
Zhang, Q., et al., 2019. Drivers of improved PM 2.5 air quality in China from 2013 to 2017. Proc. Natl. Acad. Sci. Unit. States Am. 116, 24463–24469.
Zheng, B., et al., 2018. Trends in China's anthropogenic emissions since 2010 as the consequence of clean air actions. Atmos. Chem. Phys. 18, 14095–14111.
Zou, Y., et al., 2017. Arctic sea ice, Eurasia snow, and extreme winter haze in China. Sci. Adv. 3, e1602751.